


Electromagnetic shielding tests of a permanent magnet generator

Mehmet Sarıkahya *

Social Security Institution, General Directorate of Service Delivery, Ankara, Türkiye, mehmetsh@gmail.com

Nihan Merve Sarıkahya 

The Ministry of Labor and Social Security, General Directorate of Occupational Health, Ankara, Türkiye,
nmakgul@gmail.com

Erol Kurt 

Gazi University, Technology Faculty, Department of Electrical and Electronics Engineering, Ankara, Türkiye,
ekurt@gazi.edu.tr

Submitted: 17.04.2023

Accepted: 29.07.2023

Published: 30.09.2023



* Corresponding Author

Abstract: In the present work, some tests on the electromagnetic interference issues of a new designed and constructed axial flux permanent magnet generator have been presented. The machine itself has multiple special laminated cores (i.e., 12) and 24 windings in the stator component with two active sides. Machine operates in 3 phases and uses disc type permanent magnets on two rotors at two sides in a sandwiched formation. Rotors have 32 magnets and freely rotates at the vicinity of stable stator within a certain air gap. The electromagnetic interference measurements have been realized for different distances and directions from the machine. Besides, the effects of different frequencies are also evaluated following the tests. It has been concluded that the shielding material shape is very important for the optimum shielding results.

Keywords: Axial flux, EMI, Electromagnetic interference, Generator, Material shape, Shielding

Cite this paper as: Sarıkahya, M., Sarıkahya, N.M., & Kurt, E. Electromagnetic shielding tests of a permanent magnet generator. *Journal of Energy Systems* 2023; 7(3): 290-301, DOI: 10.30521/jes.1283885

© 2023 Published by peer-reviewed open access scientific journal, JES at DergiPark (<https://dergipark.org.tr/jes>)

1. INTRODUCTION

Parallel to the increase in household and industrial electrical energy consumption, a growing demand has been given worldwide for energy conversion systems. Efficient, compact, cheap conversion machines are getting interested in the market. On the one hand, as a main wind energy equipment, generators have many types and characteristics in the market depending on their power scales and on-grid and off-grid usage.

The fact that they are noiseless, environmentally friendly, and carbonless with an efficient conversion factor, compact volume, low installation cost, and maintenance is the main idea behind the application of a wind energy conversion machine today. In this respect, wind energy applications require an optimized design with very low mechanical resistance (i.e., damping, noise, etc.). For instance, an optimized machine must meet some advantages such as high energy density, low cost, and low knock torque value [1,2]. To achieve these advantages, PMs produced from rare earth elements have an important position. The fact that they can be produced in any geometry and magnetization range and have high magnetic flux densities allows PM generators with these magnets to be widely used by the industry [3]. Axial flux generators are suitable for use in many low and medium-speed applications. This generator structure is encountered in robotics, machine parts, and electric vehicles. The reason why axial flux permanent magnet generators (AFPMGs) are well known is that

- *They are gearless formations with high torque values in the turbine component [4,5].*
- *AFPMGs can operate directly between 10 Hz and 100 Hz wind speeds and generate AC waveforms [6].*

Electromagnetic compatibility (EC) is a vital branch of electrical engineering in which the emission, production, and reception of electromagnetic energy are investigated. Electromagnetic energy can affect the operation of electronic systems and can also be harmful to living cells above a limited dose value. One of the methods used to prevent the undesired effects of electromagnetic fields and to ensure the smooth operation of electronic systems is the concept of “shielding” [7]. Today, the rapid development of electronic technology and the dependence on high-speed electronic devices and systems cause the performance of electronic and telecommunication devices such as wireless systems, television, navigation systems, mobile phones, and radar to increase [8,9,10]. Electromagnetic radiation, which emerged because of electronic developments, has brought the problem of electromagnetic pollution to the agenda. Electromagnetic Interference (EMI) shielding is expressed as controlling electromagnetic interference by blocking its radiation with barriers made of conductive or magnetic materials [11]. Methods have been tried to solve EMI problems by developing materials that absorb or reflect electromagnetic radiation in a certain frequency range. They can be used as radiation shields for sensitive electronics or to protect humans from harmful radiation [12,13,14,15,16]. An effective EMI shielding material has both high electrical conductivity and high dielectric constant, often found in metals. For these reasons, metallic sheets and thin foils are widely used as EMI shields [8,17,18].

The Shielding materials offer the ability to block and attenuate the emitted signal by back-reflecting field waves or by absorbing and dissipating the radiation power within the material. The shielding properties of these materials are determined by using the shielding efficiency (SE) parameter [11]. EMI shielding is demanded by electrical equipment, aerospace, medical and military applications. SE is measured in decibels (DB) and is a commonly used parameter for determining shielding performance. These materials are used in the shell of electronic equipment or as a body shell at the entrance of electromagnetic waves and prevent electromagnetic leakage [19,20,21].

In this work, we analyze the EMI and shielding features of a new designed and constructed AFPMG. The fundamental of EMI is given in next section. Measurement methods and characteristics of the cages

used are given in Section 3. The experimental results and main discussion are given in Section 4. Finally, the paper ends with the concluding remarks.

2. MATERIALS AND METHODS

Fig. 1 shows the components creating the shielding effect. Electromagnetic waves are attenuated in three ways in shielding materials. The first is reflections from the wall.

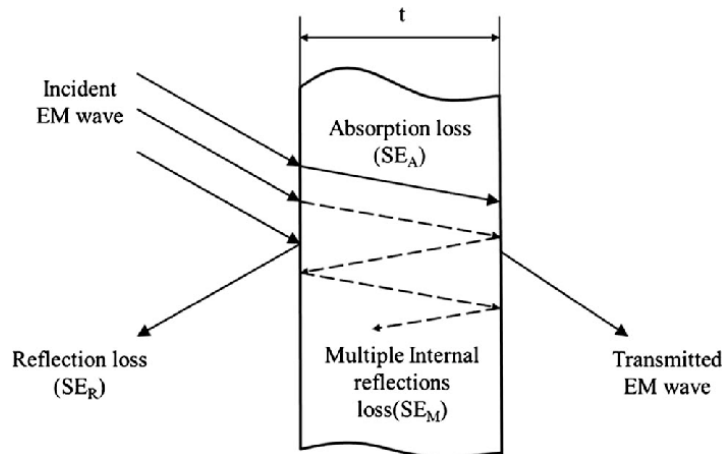


Figure 1. Attenuation of an electromagnetic wave by a shield

The second is attenuation due to the absorption in the wall. The third is sequential reflection losses inside the wall. The shielding performance depends on the properties of the materials. The SE can thereby be expressed as the sum of three contributions [22,23,24] as shown in Eq. (1).

$$SE = SE_R + SE_A + SE_M \quad (1)$$

Here reflection and absorption losses and the multiple reflection are given by SE_R , SE_A and SE_M , respectively as shown in Eq. (2-5).

$$SE_R = 10 \log \left[\frac{\sigma_r}{16\omega\epsilon_0\mu_r} \right] \quad (2)$$

$$\delta = 2,6/\sqrt{f\mu_r\sigma_r} \quad (3)$$

$$SE_A = 3,34t\sqrt{f\mu_r\sigma_r} = 8,68 \frac{t}{\delta} \quad (4)$$

$$SE_M = 20 \log(1 - e^{-2t/\delta}) \quad (5)$$

where δ is the depth of the material, f is the frequency, σ is the electrical conductivity, μ is the magnetic permeability of the shield materials and t is the thickness of the shield materials.

E and H represent electric and magnetic fields, P represent power of the waves as shown in Eq. (6-8) respectively. t and i represent transmitted and incoming waves.

$$SE = 20 \log(E_i/E_t) \quad (6)$$

$$SE = 20 \log(H_i/H_t) \quad (7)$$

$$SE = 20 \log(P_i/P_t) \quad (8)$$

Within the frame of present work, the electromagnetic field measurements are obtained by using a Wavecontrol SMP2 device as shown in Fig. 2.



Figure 2. Wavecontrol SMP2 device [24].

The SMP2 is a device with a range of compatible probes from 1 Hz to 40 GHz, used to measure electromagnetic fields. The SMP2 was developed to meet the needs of personal safety assessments in connection with exposure to electromagnetic fields and can be used in many different sectors and industries. In this study, WP400 probe was chosen. The main reason for this is the field measurements are between 1 Hz - 400 kHz and E/H is selected as the field.

2.1. Measurement Method

Determining the attenuation level of an EMI shield can be complex and research methods often vary with the particular shield application [25]. In addition to material properties such as conductivity and permeability, many factors such as frequency, place of measurement, polarization, and incidence angle of the striking wave, near field or far field application affect EMI SE. There are many techniques to measure the EMI SE value [26]: The prominent ones are first, coaxial transmission line method, second, shielded box method, third, rectangular waveguide method, etc.

In this work, the frequency domain measurement (i.e., FFT) method is chosen because the EM field depending on the frequency is important in our case. Fig. 3 presents a sample FFT measurement.

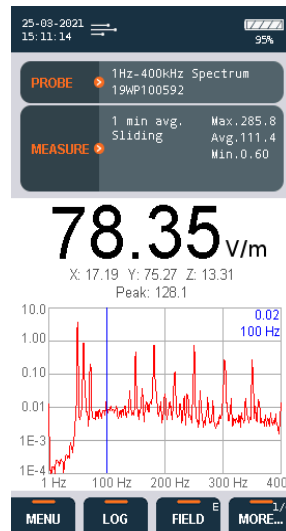


Figure 3. A sample FFT mode measurement

Note that this mode is only available under a selective probe of WP400, WP400-3 or the WPH-DC. The Frequency domain measurements include the frequency information on the analyzed field following the calculation on the FFT. Since the analyzes are performed at 1 kHz - 400 kHz frequencies with the FFT method, the EM field measurements are carried out by using the Wavecontrol SMP2 WP400 model.

2.2. Characteristics of the Cages

The setup for the laboratory tests is shown in Fig. 4. The experimental unit basically includes a controller unit which enables us to adjust the rotor speed, an induction motor which drives the proposed AFPMG, coupling units for the AFPMG and electrical loads.

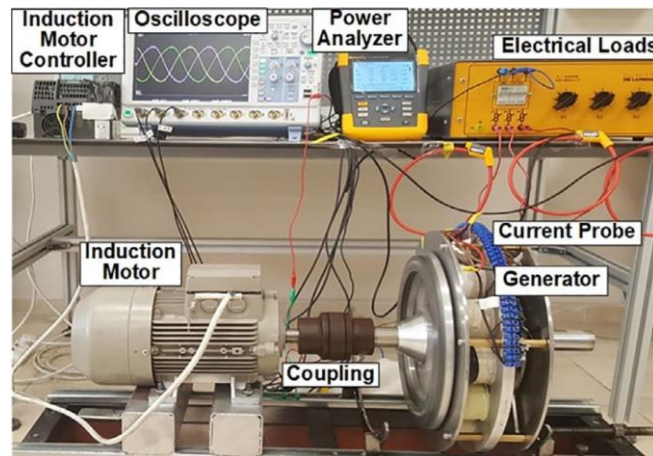


Figure 4. The setup for the electrical measurements of the proposed machine [3].

According to workflow, three cages with different features have been used for the EM shielding. Initially, the generator is operated without any electrical load. It means that from the generator any electrical current is flowed. That is important for background radiation measurements. Later, the loads are attached, and the measurements have been repeated while an electrical current flows from the windings. At this stage, the measurements are performed with 3 cages namely swatter, honeycomb and square from various distances of 10 cm, 20 cm, and 30 cm from the cages. The swatter material used as shielding is wire mesh with a diameter of 1 mm and consists of stainless steel. The honeycomb material used as shielding is wire mesh with a diameter of 10 mm and consists of steel. The Square material is wiring mesh with a diameter of 5 mm and consists of steel. The characteristics of the cages are given in the Figs. 5-7.

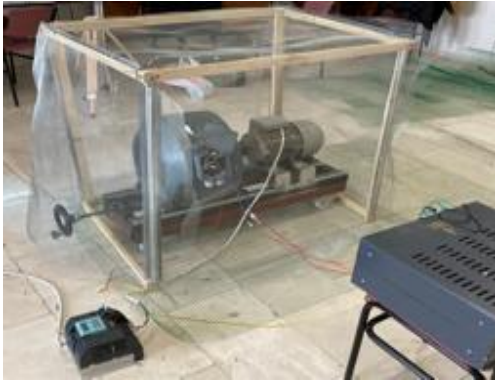


Figure 5. Shielding material of swatter type.

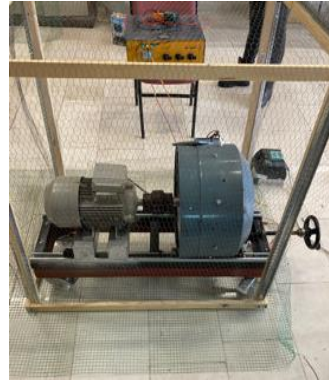


Figure 6. Shielding material of honeycomb type.

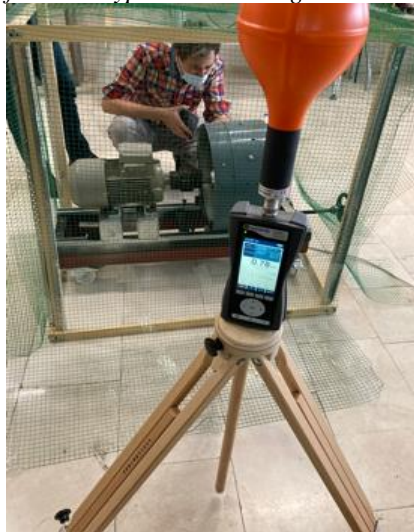


Figure 7. Shielding material of square type.

3. EXPERIMENTAL RESULTS AND DISCUSSION

The tests are completed for three metal cages with the dimensions of 10 cm, 20 cm and 30 cm. From 100 rpm to 1100 rpm rotation speed of the AFPMG, we have performed the tests. These values generate waveforms from $f= 20$ Hz to 30 Hz. Note that the measurement probe has been used from different sides of the cage (i.e., front, right, left, back, top). The relationship of frequency and rotor speed is shown in Fig. 8.

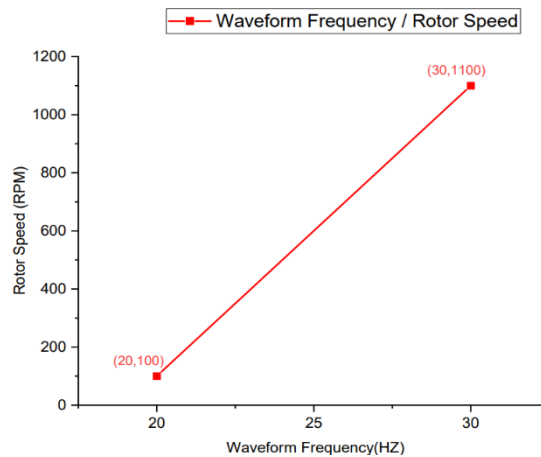


Figure 8. The frequency and rotor speed relation of the AFPMG.

Figs. 9,10,11,12,13(a,b) give the overall electromagnetic characteristics of AFPMG from the front, right, back, left, and top sides at different waveform frequencies (i.e. 20 Hz and 30 Hz). According to the tests, when the distance from the cage is increased, it has been proven that the EM values (i.e., E and H) for all regions decrease. Note that when the rotor speed increases from 100 rpm to 1000 rpm, the EM parameters substantially increase on each surface. It is observed that the EM values increase linearly with rotor speed for all 3D plots.

Figs. 9(a,b) gives the overall electromagnetic characteristics of the AFPMG from the front side. The highest electromagnetic values for both 20 Hz and 30 Hz waveform frequencies are obtained for the square cage. From the front side at 20 Hz waveform frequency (i.e., 100 rpm for rotor speed), for all distances (as a sum over all distances) 10 cm, 20 cm, and 30 cm, the electric field is found to be 22.64 V/m for square, 606.3 V/m for null, 209.86 V/m for honeycomb, 106.5 V/m for swatter.

Under $f=30$ Hz waveform frequency (i.e., 1100 rpm for rotor speed), for the square shielding, while E is measured as 93.18 V/m. E is 724.1 V/m for null, 295.86 V/m for honeycomb, and 134.63 V/m for swatter. Note that these values are the sum of the values for 10 cm, 20 cm, and 30 cm distances. These values indicate the maximal value on the null and 10 cm of the distance as 308.3 V/m, whereas the minimum is obtained at square shielding at 30 cm of the distance with 1.8 V/m. In addition, the electric field strength is found to be higher for 30 Hz than 20 Hz waveform frequencies. The reason for the high values measured on the front face is that the load connections and connectors are connected from this side.

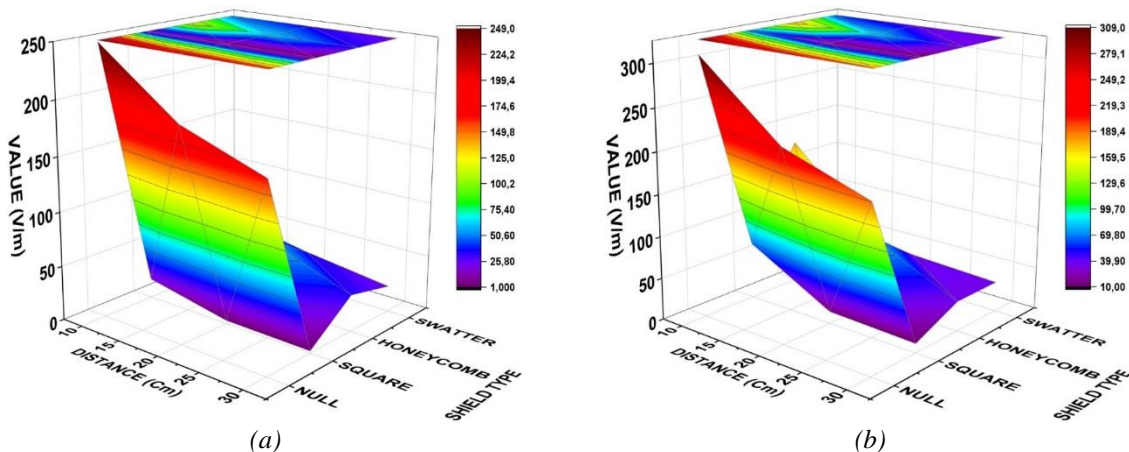


Figure 9. Electric field from the front side: (a) $f=20$ Hz waveform frequency, (b) $f=30$ Hz waveform frequency.

Figs. 10(a,b) shows the overall electromagnetic characteristics of the AFPMG from right side. The highest electric field values are measured as 20 Hz and 30 Hz waveform frequencies for the swatter cage. Strictly speaking, at 20 Hz waveform, the sum of 10 cm, 20 cm, 30 cm distances are found for swatter cage. Besides, while it is 3.09 V/m for swatter cage, 448.21 V/m is found for null, 76.2 V/m is measured for honeycomb cage and 9.16 V/m is obtained for the square cage. In the case of high rotation rate (i.e. 30 Hz waveform rotor speed), the sum of 10 cm, 20 cm and 30 cm distances for the swatter cage is 4.86 V/m. $E= 510.7$ V/m, $E=142.97$ V/m and $E=25.69$ V/m are measured for null, honeycomb and square cages respectively. Note that these are also sum of values obtained at 10 cm, 20 cm, 30 cm of distances. The maximum value on the null at 10 cm of the distance with $E= 258.7$ V/m. The minimum is found for the swatter cage at 30 cm of the distance with $E= 0.7$ V/m. Meanwhile, the field values are larger for 30 Hz waveform frequencies compared to the case for 20 Hz waveform frequency.

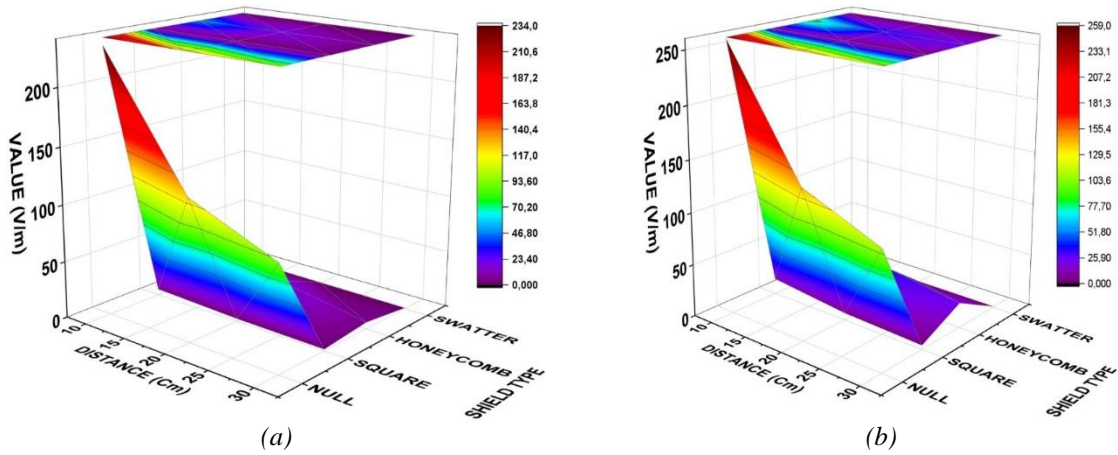


Figure 10. Electric field from the right side: (a) $f=20$ Hz waveform frequency, (b) $f=30$ Hz waveform frequency.

Figs. 11(a, b), gives the overall electromagnetic characteristics of the AFPMG from back side. The highest electromagnetic values for both 20 Hz waveform frequency (i.e. 100 rpm for rotor speed), 30 Hz waveform frequency (i.e. 1100 rpm for rotor speed), obtained for the swatter cage. For the back side; at 20 Hz waveform frequency, while it was 2.14 V/m for swatter, $E=402.44$ V/m for null, $E=20.78$ v/m for honeycomb, $E=24.81$ v/m for square. At 30 Hz waveform frequency, while it was 2.53 V/m for swatter, $E=514.4$ V/m for null, $E=76.09$ V/m for honeycomb, $E=38.84$ V/m for square. Note that these values are the sum of values 10, 20, 30 cm of distance. These values indicate the maximal value on the null and 10 cm of the distance as 208.6 V/m. However, the minimal value on swatter at 30 cm of the distance as 0.5 V/m. At the same time; it can be observed that the electromagnetic value is higher for $f=30$ Hz than $f=20$ Hz.

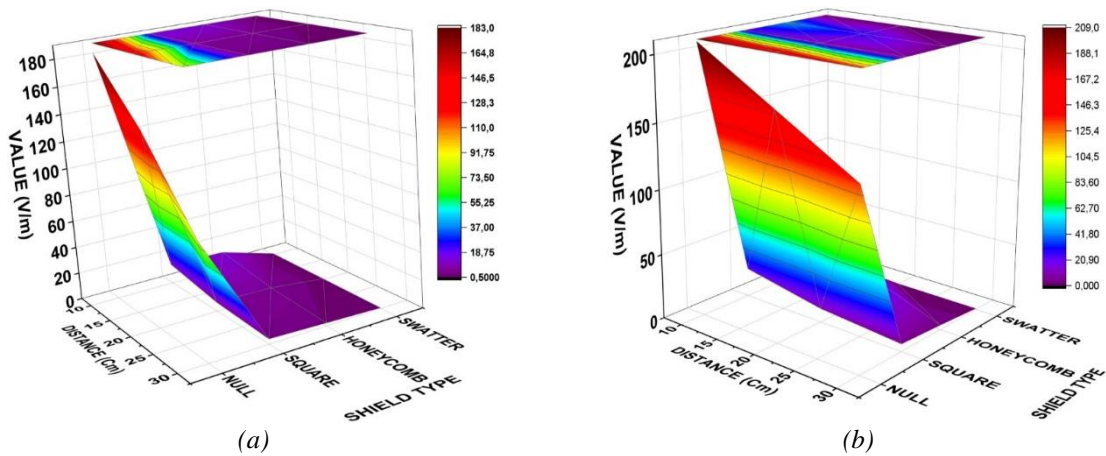


Figure 11. Electric field from the back side: (a) $f=20$ Hz waveform frequency, (b) $f=30$ Hz waveform frequency

Figs. 12 (a, b), gives the overall electromagnetic characteristics of the AFPMG from left side. The highest electromagnetic values for 20 Hz waveform frequency (i.e., 100 rpm for rotor speed) and 30 Hz waveform frequency (i.e., 1100 rpm for rotor speed) obtained for the swatter cage. For the back side, at 20 Hz waveform frequency, while it was 6.44 V/m for swatter, $E= 530.8$ V/m for null, $E=95.74$ V/m for honeycomb, $E=30.6$ V/m for square. At 30 Hz waveform frequency, while it was 15.79 V/m for swatter, $E=562.8$ V/m for null, $E=217.72$ V/m for honeycomb, $E=37.72$ V/m for square. Note that these values are the sum of values 10 cm, 20 cm and 30 cm of distances.

These values indicate the maximal value on the null and 10 cm of the distance as 252.9 V/m. However, the minimal value on swatter at 30 cm of the distance as 1.2 V/m. At the same time; it can be observed that the electromagnetic value is higher for $f=30$ Hz than $f=20$ Hz.

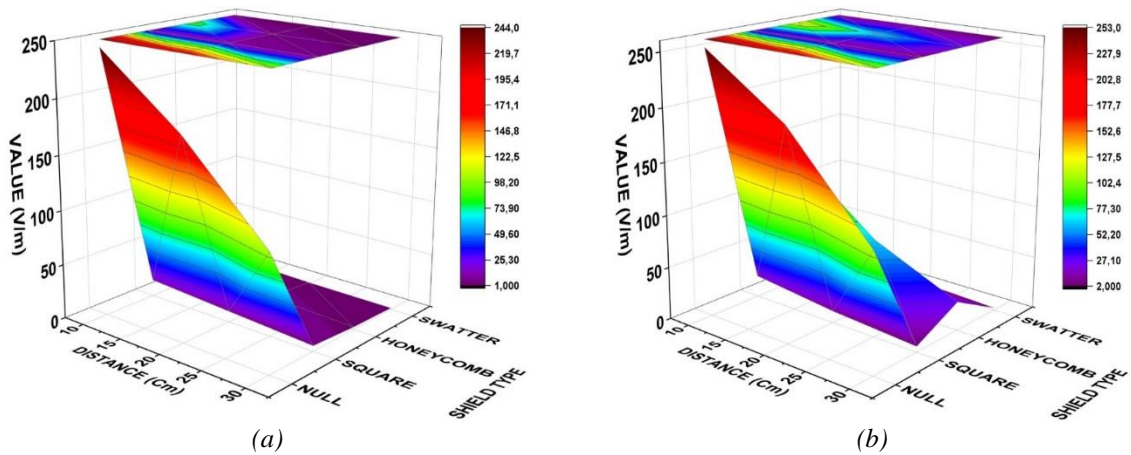


Figure 12. Electric field from the left side: (a) $f=20$ Hz waveform frequency, (b) $f=30$ Hz waveform frequency

Figs. 13 (a,b), gives the overall electromagnetic characteristics of the AFPMG from top side. The highest electromagnetic values for both 100 rpm and 1100 rpm for rotor speed obtained for the swatter cage. For the top side; at 20 Hz waveform frequency, while it was 7.19 V/m for swatter, $E=325.65$ V/m for null, $E=34$ V/m for honeycomb, $E=13.86$ V/m for square. At 30 Hz waveform frequency, while it was 9.94 V/m for swatter, $E=441.95$ V/m for null, $E=51.29$ V/m for honeycomb, $E=22.75$ V/m for square. Note that these values are the sum of values 10, 20, 30 cm of distances.

These values indicate the maximal value on the null and 10 cm of the distance as 216.1 V/m. However, the minimal value on swatter at 30 cm of the distance as 1.19 V/m. At the same time; it can be observed that the electromagnetic value is higher for $f=30$ Hz than $f=20$ Hz.

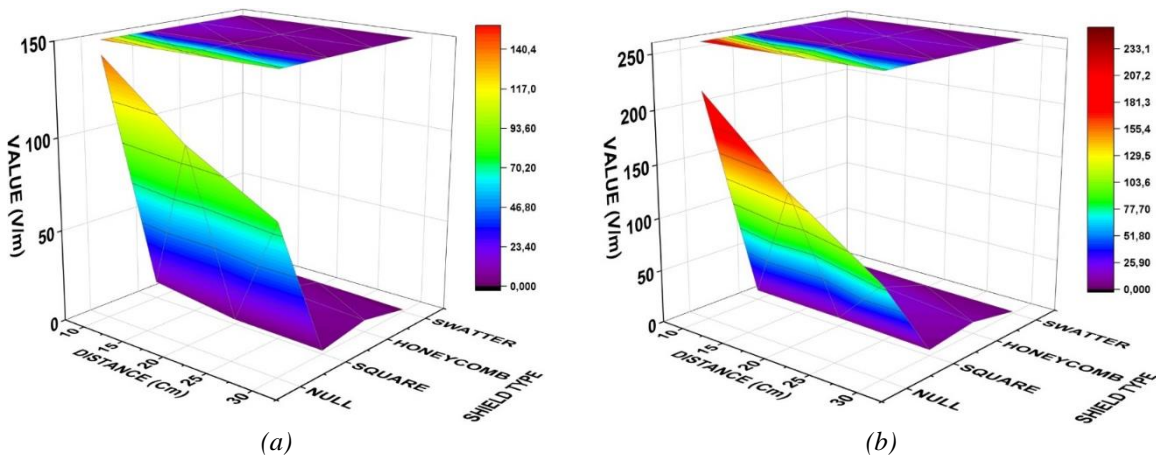


Figure 13. Electric field from the top side: (a) $f=20$ Hz waveform frequency, (b) $f=30$ Hz waveform frequency.

The results of the simulations for outer and inner electromagnetic fields are given in Fig. 14. In the case of no shielding at null, the highest values of outer electromagnetic fields were reached as seen in the fig. 14, and the value of 248 V/m was measured at 30 Hz and at a distance of 10 cm. It was observed that after the shielding application, the electromagnetic field decreased linearly on the outside and reached the lowest value of 11.5 V/m for the swatter at 20 Hz. In contrast to the external electromagnetic field, it is seen in fig. 14 that the inner electromagnetic field inside the cage increases linearly. In accordance with the theory, as the shielding increases, the power of the electromagnetic wave reflected inside the cage increases and this causes the electromagnetic field value measured inside to increase. As seen in Fig. 14, the highest inner electromagnetic field value was reached at $f=30$ Hz in the swatter.

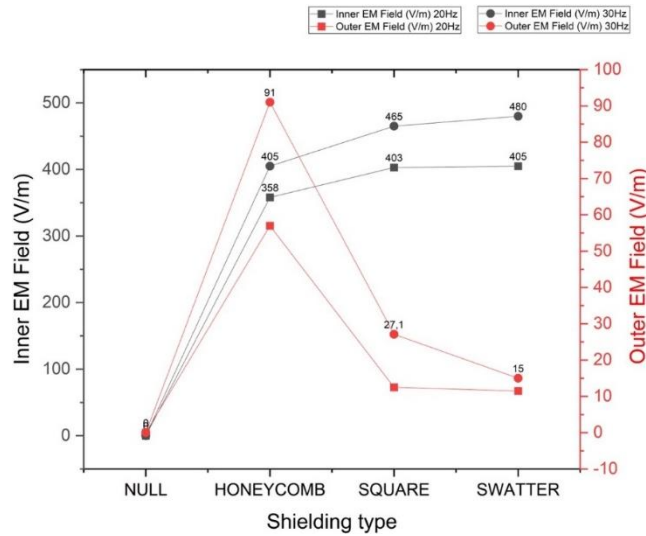


Figure 14. Outer electromagnetic field, distance of 10 cm and inner electromagnetic field of cages.

Fig. 15 summarizes the SE value at $f=20$ Hz and $f=30$ Hz for 3 different shielding variants. As seen in Fig. 15, the highest shielding value is provided by the swatter at different waveform frequencies. A shielding value of over 25 dB is provided for the swatter at 20 Hz and 30 Hz. On the contrary, 16 dB and 8.7 dB SE values were obtained for the honeycomb for $f=20$ Hz and $f=30$ Hz, respectively. Considering that the material used for the swatter is stainless steel, unlike honeycomb and square, it is seen that shielding will be much better if a material with higher conductivity is used. The fact that the diameter of the swatter screen material is smaller than the honeycomb and square seems to be an important factor in obtaining the best SE value. In conclusion, a material with an attenuation level between 90 dB and 120 dB is considered to have excellent shielding performance. Any calculated attenuation greater than 100 dB means that the material is essentially impenetrable [11]. Indeed, $SE \leq 10$ dB is assigned to weak, 10-30 dB is assigned to acceptable and $SE \geq 30$ dB is assigned to the exceeding the acceptable value of 20 dB for industrial and commercial applications [23].

The shielding analyzed, having a shielding effectiveness above 25 dB for swatter, provide a significant degree of attenuation of the electromagnetic radiation.

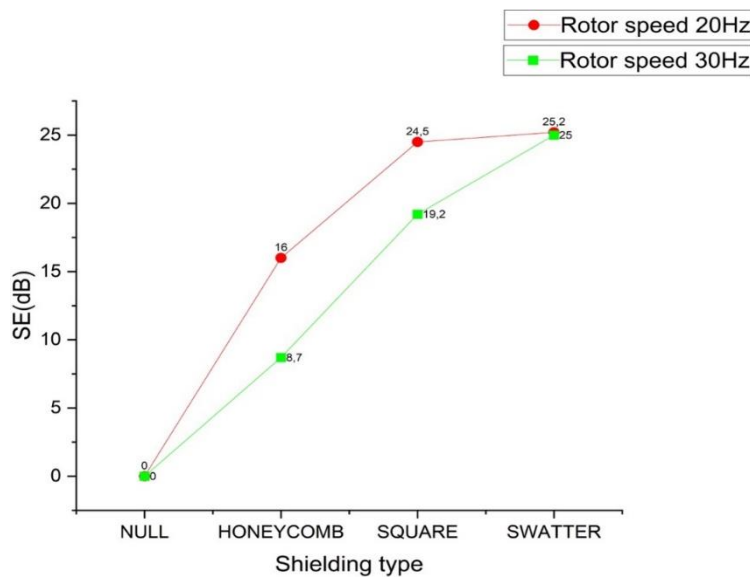


Figure 15. Shielding effectiveness results of AFPMG.

4. CONCLUSION

This work performs axial flux permanent magnet generator electromagnetic interference measurement. Initially, commonly used measurement techniques are mentioned. The tests prove that the swatter cage material provides the best shielding effectiveness for the generator from all the rotor speeds. While the field decreases with distance from the cage, good shielding effectiveness has been noted compared to the no-shielding cases. The information disclosed in this paper is focused on the EMI shielding efficiency of AFPMG and the calculation of the SE parameter of the three shielding materials. The results of the experimental tests demonstrate a significant ability to block electromagnetic radiation. For Honeycomb, SE values of 16 dB and 8.7 dB were obtained for $f=20$ Hz and $f=30$ Hz waveform frequencies, respectively. For the second shielding method, square; 24.5 dB and 19.2 dB SE values were obtained for 20 Hz and 30 Hz waveform frequencies, respectively, and for the last method, swatter; SE values of 25.2 dB and 25 dB were obtained for 20 Hz and 30 Hz waveform frequencies, respectively. It has been concluded that the SE value of the swatter shielding is over 25 dB at all measuring distances and at different frequencies and has better performance than honeycomb and square shielding.

Acknowledgment

This research was supported by the Scientific and Technological Research Council of Turkey (TUBITAK) under Grant No. MAG-315M483.

REFERENCES

- [1] Gor, H, Kurt, E. Preliminary studies of a new permanent magnet generator (PMG) with the axial and radial flux morphology. *International Journal of Hydrogen Energy* 2016; 41: 7005-7018. DOI: 10.1016/j.ijhydene.2015.12.195
- [2] Bouloukza, I, Mordjaoui, M, Kurt, E, Bal, G, Ökmen, C. Electromagnetic design of new radial flux permanent magnet motor. *Journal of Energy Systems* 2018; 2(1): 13- 27. DOI: 10.30521/jes.397836
- [3] Kurt, E, Gör, H, Çelik, K. Optimization of a 3-kW axial flux permanent magnet generator with variable air gap. *Int Trans Electr Energy Syst.* 2021; 31(11): e13074. DOI: 10.1002/2050-7038.13074
- [4] Yıldırım, E, Aydemir, MT. Analysis, design and implementation of an axial flux, permanent magnet machine to be used in a low power wind generator. *J Fac Eng Archit Gazi Univ* 2009; 24(3): 525-31.
- [5] Celik, E, Gor, H, Ozturk, N, Kurt E. Application of artificial neural network to estimate power generation and efficiency of a new axial flux permanent magnet synchronous generator. *international journal of hydrogen energy* 2017; 42(28): 17692-17699. DOI: 10.1016/j.ijhydene.2017.01.168
- [6] Kurt, E, Gör, H, Demirtas, M. Theoretical and experimental analyses of a single-phase permanent magnet generator (PMG) with multiple cores having axial and radial directed fluxes. *Energ Conver Manage.* 2014; 77: 163-172. DOI: 10.1016/j.enconman.2013.09.013
- [7] Neruda, M, Vojtech, L. Electromagnetic shielding effectiveness of woven fabrics with high electrical conductivity: complete derivation and verification of analytical model. *Materials* 2018; 11(9): 1657. DOI: 10.3390/ma11091657
- [8] ASTM Standard D4935, In Standard Test Method for Measuring the Electromagnetic Shielding Effectiveness of Planar Materials; ASTM International: West Conshohocken, PA, USA, 2010.
- [9] Viskadourakis, Z, Vasilopoulos, KC, Economou, EN. Electromagnetic shielding effectiveness of 3D printed polymer composites. *Applied Physics A* 2017; 123: 736. DOI: 10.1007/s00339-017-1353-z
- [10] Çelik, K, Kurt, E. Design and implementation of a dual band bioinspired leaf rectenna for RF energy harvesting applications. *Int. J. RF & Microwave Computer-Aided Engineering* 2021; 31(11): e22868. DOI: 10.1002/mmce.22868.
- [11] Munalli, D, Dimitrakis, G, Chronopoulos, D. Electromagnetic shielding effectiveness of carbon fibre reinforced composites. *Composites Part B* 2019; 173: 106906. DOI: 10.1016/j.compositesb.2019.106906
- [12] Celozzi, S, Araneo, R. Electromagnetic Shielding. In *Encyclopedia of RF and Microwave Engineering*, Chang, K, Editor. DOI: 10.1002/0471654507.eme094
- [13] Kuester, S, Demarquette, NR. Hybrid nanocomposites of thermoplastic elastomer and carbon nanoadditives for electromagnetic shielding. *European Polymer Journal* 2017; 88: 328-339. DOI: 10.1016/j.eurpolymj.2017.01.023

- [14] Yao, Y, Zhao, J, Yang, X, Chai, C. Recent advance in electromagnetic shielding of Mxenes. *Chinese Chemical Letters* 2021; 32(2): 620-634. DOI: 10.1016/j.ccl.2020.07.029
- [15] Pan, T, Zhang, Y, Wang, C, Gao, H, Wen, B, Yao, B. Mulberry-like polyaniline-based flexible composite fabrics with effective electromagnetic shielding capability. *Composites Science and Technology* 2020; 188: 107991. DOI: 10.1016/j.compscitech.2020.107991
- [16] Khodiri, AA, Al-Ashry, MY, El-Shamy, AG. Novel hybrid nanocomposites based on polyvinyl alcohol/graphene/magnetite nanoparticles for high electromagnetic shielding performance. *Journal of Alloys and Compounds* 2020; 847: 156430. DOI: 10.1016/j.jallcom.2020.156430
- [17] Zhan, Y, Long, Z, Wan, X. 3D carbon fiber mats/nano-Fe₃O₄ hybrid material with high electromagnetic shielding performance. *Applied Surface Science* 2018; 444: 710-720. DOI: 10.1016/j.apsusc.2018.03.006
- [18] Zhu, H, Yang, Y., Sheng, A. Layered structural design of flexible waterborne polyurethane conductive film for excellent electromagnetic interference shielding and low microwave reflectivity. *Applied Surface Science* 2019; 469: 1-9. DOI: 10.1016/j.apsusc.2018.11.007
- [19] Liu, L, Chen, X, Jingfeng W. Effects of Y and Zn additions on electrical conductivity and electromagnetic shielding effectiveness of Mg-Y-Zn alloys. *Journal of Materials Science and Technology* 2019; 35(6): 1074-1080. DOI:10.1016/j.jmst.2018.12.010
- [20] Wanasinghe, D., Aslani, F, Ma, G. Electromagnetic shielding properties of carbon fibre reinforced cementitious composites. *Construction and Building Materials* 2020; 260: 120439. DOI: 10.1016/j.conbuildmat.2020.120439
- [21] Wang, Y, Wanga, W, Dinga, X. Multilayer-structured Ni-Co-Fe-P/polyaniline/polyimide composite fabric for robust electromagnetic shielding with low reflection characteristic. *Chemical Engineering Journal* 2020; 380: 122553. DOI: 10.1016/j.cej.2019.122553
- [22] Wypych, G. Handbook of Fillers: Pigment & Resin Technology, Vol. 28 No. 2, 1999.
- [23] Afilipoaei, C, Teodorescu-Draghicescu, H. A review over electromagnetic shielding effectiveness of composite materials. *Proceedings* 2020; 63: 23. DOI: 10.3390/proceedings2020063023
- [24] SMP2, Technical manuel, (2022).
- [25] Safarova, V, Militky, J. Multifunctional metal composite textile shields against electromagnetic radiation effect of various parameters on electromagnetic shielding effectiveness. *Polymer Composites* 2017; 38(2): 309–323. DOI: 10.1002/pc.23588
- [26] Mathur, P, Raman, S. Electromagnetic interference (EMI): measurement and reduction techniques. *Journal of Electronic Materials* 2020; 49: 2975–2998. DOI:10.1007/s11664-020-07979-1